Nanoscale

ROYAL SOCIETY OF CHEMISTRY

PAPER

View Article Online
View Journal | View Issue

Cite this: *Nanoscale*, 2020, **12**, 9423

Ligand exchange on $Au_{38}(SR)_{24}$: substituent site effects of aromatic thiols†

Yingwei Li,[a] Rosalba Juarez-Mosqueda,[b] Yongbo Song,[c] Yuzhuo Zhang,[a] Jinsong Chai,[a] Giannis Mpourmpakis *[b] and Rongchao Jin *[a]

Received 19th February 2020,
Accepted 21st March 2020

DOI: 10.1039/d0nr01430c

rsc.li/nanoscale

Understanding the critical roles of ligands (*e.g.* thiolates, SR) in the formation of metal nanoclusters of specific sizes has long been an intriguing task since the report of ligand exchange-induced transformation of $Au_{38}(SR)_{24}$ into $Au_{36}(SR')_{24}$. Herein, we conduct a systematic study of ligand exchange on $Au_{38}(SC_2H_4Ph)_{24}$ with 21 incoming thiols and reveal that the size/structure preference is dependent on the substituent site. Specifically, *ortho*-substituted benzenethiols preserve the structure of $Au_{38}(SR)_{24}$, while *para*- or non-substituted benzenethiols cause its transformation into $Au_{36}(SR)_{24}$. Strong electron-donating or -withdrawing groups do not make a difference, but they will inhibit full ligand exchange. Moreover, the crystal structure of $Au_{38}(SR)_{24}$ (SR = 2,4-dimethylbenzenethiolate) exhibits distinctive π···π stacking and "anagostic" interactions (indicated by substantially short Au···H distances). Theoretical calculations reveal the increased energies of frontier orbitals for aromatic ligand-protected Au_{38}, indicating decreased electronic stability. However, this adverse effect could be compensated for by the Au···H–C interactions, which improve the geometric stability when *ortho*-substituted benzenethiols are used. Overall, this work reveals the substituent site effects based on the Au_{38} model, and highlights the long-neglected "anagostic" interactions on the surface of Au-SR NCs which improve the structural stability.

1 Introduction

Ligand-protected metal nanoclusters (NCs) of atomic precision have been of interest to researchers not only because of their unusual properties due to quantum confinement and structural diversity, but also because of the opportunity to correlate the structures and the properties.[1,2] Thiols (HSR) are the most widely used ligands in producing Au NCs owing to strong Au–S bonds. In the early works by the Tsukuda group,[3–5] a series of glutathione-protected $Au_n(SR)_m$ were separated and identified by mass spectrometry (MS). To obtain the total structures *via* single-crystal X-ray diffraction, organic ligands were devised to achieve crystallization; for example, the structures of $Au_{25}(SR)_{18}$ and $Au_{38}(SR)_{24}$ were successfully obtained with the help of 2-phenylethanethiol (PET),[6–8] and cyclohexanethiol was used to crystallize $Au_{18}(SR)_{14}$.[9,10] It was later found that 4-*tert*-butylbenzenethiol (TBBT, the same abbreviation for the thiolate form) could give rise to a series of Au-SR NCs with face-centered cubic kernels,[11] while *tert*-butylthiol was used to synthesize Au_{23}, Au_{30}, Au_{46} and Au_{65}.[12] For alloy NCs, the $[Au_{12+n}Cu_{32}(SR)_{30+n}]^{4-}$ series (n = 0, 2, 4, and 6) were prepared using 4-(trifluoromethyl)thiophenol,[13] whereas adamantanethiol produced a series of Au/Ag alloy clusters of structural differentiation *via* asymmetric Ag doping.[14]

In addition, the bulkiness of ligands was found to control the size of Au-SR NCs,[15] and the position of substituents on benzenethiolate ligands is also decisive as $Au_{130}(SR)_{50}$, $Au_{104}(SR)_{41}$, and $Au_{40}(SR)_{24}$ NCs were achieved by isomeric *para*-, *meta*-, and *ortho*-methylbenzenethiols, respectively.[16] The Ag_{16} and Ag_{32} NCs were prepared using 3,4-difluorothiophenol and 4-(trifluoromethyl)thiophenol, respectively,[17] whereas 2,4- and 2,5-dimethylbenzenethiols resulted in Ag_{40} and Ag_{46}, respectively.[18] Such a size/structure selectivity dictated by different ligands is also demonstrated by ligand exchange,[19–23] implying that a specific thiol would have its preference for certain magic-sizes of metal-SR NCs over other sizes.

The ligand effect on Au NCs was also studied theoretically.[24–26] Based on the early models derived from $[Au_{25}(SR)_{18}]^-$, $Au_{38}(SR)_{24}$, and $Au_{102}(SR)_{44}$, it has been reported that the aliphatic thiolate-stabilized NCs have higher electrochemical and thermodynamic stability than their aromatic

[a]*Department of Chemistry, Carnegie Mellon University, Pittsburgh, Pennsylvania 15213, USA. E-mail: rongchao@andrew.cmu.edu*
[b]*Department of Chemical Engineering, University of Pittsburgh, Pittsburgh, Pennsylvania 15261, USA. E-mail: gmpourmp@pitt.edu*
[c]*Department of Chemistry and Centre for Atomic Engineering of Advanced Materials, Anhui Province Key Laboratory of Chemistry for Inorganic/Organic Hybrid Functionalized Materials, Anhui University, Hefei, Anhui 230601, People's Republic of China*

†Electronic supplementary information (ESI) available. See DOI: 10.1039/d0nr01430c

thiolate-stabilized counterparts.[24] Density functional theory (DFT) analyses provided insights into the isomer stability of $Au_{24}(SR)_{20}$ and $Au_{28}(SR)_{20}$.[26–28]

The geometric/electronic structures of Au_{38} NCs and their properties have been studied for years.[29–32] Motivated by the importance of ligands in associating specific sizes based on their stability, herein we conduct a systematic ligand exchange study on $Au_{38}(PET)_{24}$ with 21 thiols and illustrate how the substituent sites on aromatic thiols affect the structural stability of Au_{38}. Additionally, the crystal structure of $Au_{38}(2,4DMBT)_{24}$ shows significant π···π interactions between phenyl rings, and more importantly "anagostic" interactions (*i.e.*, Au···H–C) are also identified. Time-dependent DFT (TDDFT) calculations show an overall increase in energy for the electronic states of aromatic ligand-protected Au_{38}, indicating reduced electronic stability; however, this disadvantage can be offset by the "anagostic" interactions. This work demonstrates the effect of *ortho*-substituents on SPh in retaining the structure of Au_{38} by forming additional Au···H–C interactions.

2 Results and discussion

The synthesis of $Au_{38}(PET)_{24}$ is based on the literature.[7] As for the ligand exchange, 1 mg of pure $Au_{38}(PET)_{24}$ was dissolved in 1 mL of toluene and then mixed with ~1 mg or ~1 μL of different incoming ligands (Scheme 1). The reactions were conducted at different temperatures (see sections below). The product was washed repeatedly using methanol, and extracted using dichloromethane. In the following sections, the acronyms for ligands (the same for the thiol and thiolate forms) are used as defined in Scheme 1.

2.1 Ligand exchange by benzenethiols with *ortho*-substituents

We first discuss the ligand exchange with *ortho*-substituted benzenethiols. Time-dependent UV-vis absorption spectra and the corresponding MALDI MS spectra (Fig. S1†) show that 2-methylbenzenethiol (2MBT) or 1-naphthalenethiol (1SNap) cannot completely replace PET on $Au_{38}(SR)_{24}$ at room temperature. However, at 80 °C, pure $Au_{38}(2MBT)_{24}$ and $Au_{38}(1SNap)_{24}$ were obtained. It should be noted that the highest peak in the MS spectrum corresponds to $Au_{38}(PET)_{24}$, while for conjugated thiolate-protected Au_{38} NCs one ligand is detached from the clusters, and the fragment by losing $Au_4(SR)_4$ becomes more prominent (Fig. S1C and F†).

The experiments were then set at 45 °C for ligand exchange with more types of *ortho*-substituted benzenethiols (Fig. S2†). It was found that moderate heating is enough for full exchange with 1SNap, 2MBT, 2,4-dimethylbenzenethiol (2,4DMBT), 2-ethylbenzenethiol (2EBT), 2,5-dimethylbenzenethiol (2,5DMBT), and 2,6-dimethylbenzenethiol (2,6DMBT), according to the MALDI-MS spectra (Fig. 1). However, the trials with 2-methyl-5-*tert*-butylbenzenethiol (2M,5TBBT), 2-fluorobenzenethiol (2FBT) and 2-methoxybenzenethiol (2MOBT) were not complete, evidenced by the formation of $Au_{38}(SR)_{23-x}(PET)_x$; we even repeated the three experiments at 80 °C (Fig. S3†), in which the number of exchanged ligands was increased, but the NCs became unstable.

Therefore, it is clear that as long as the incoming thiol has an *ortho*-substituted group on the phenyl ring, $Au_{38}(SR)_{24}$ is favored. However, when a bulky group (*e.g.* the ^{t}Bu group), a strong electron-donating (–OCH_3) or -withdrawing (–F) group, is involved, the ligand exchange will be disturbed.

2.2 Ligand exchange by benzenethiols with *meta*-/*para*-substituents

Based on the results from *ortho*-substituted benzenethiols, we then conducted the ligand exchange with *para*- or *meta*-substituted benzenethiols, including 2-naphthalenethiol (2SNap), 4-methylbenzenethiol (4MBT), 3,4-dimethylbenzenethiol (3,4DMBT), 4-ethylbenzenethiol (4EBT), 4-*tert*-butyl-benzenethiol (TBBT), 4-fluorobenzenethiol (4FBT), 4-methoxybenzenethiol (4MOBT), 3-methylbenzenethiol (3MBT) and 3,5-dimethylbenzenethiol (3,5DMBT), at room temperature (RT) (Fig. S4†). Although ligand exchange was incomplete at RT, $Au_{38}(SR)_{24}$ NCs protected by mixed thiols were observed to be the only products (Fig. 2), whereas higher temperatures would induce structural transformation (*vide infra*). It should be noted that because 3,4DMBT and 4EBT have the same molecular weights as that of PET, the number of incoming ligands cannot be determined by MS, but it should be similar to that of 2SNap or 4MBT. $Au_{38}(TBBT)_{23-x}(PET)_x$ NCs show identical characteristics to those of the intermediate formed during the preparation of $Au_{36}(TBBT)_{24}$ in previous work.[21]

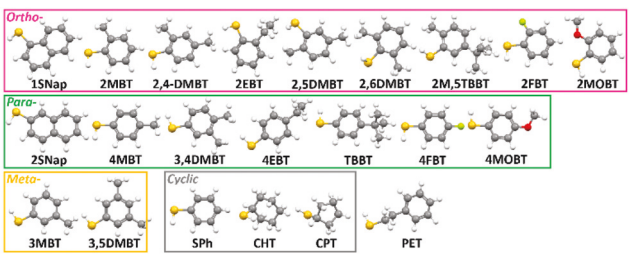

Scheme 1 The thiols used in ligand exchange with $Au_{38}(PET)_{24}$. Color code: yellow = S; grey = C; white = H; red = O; and light green = F.

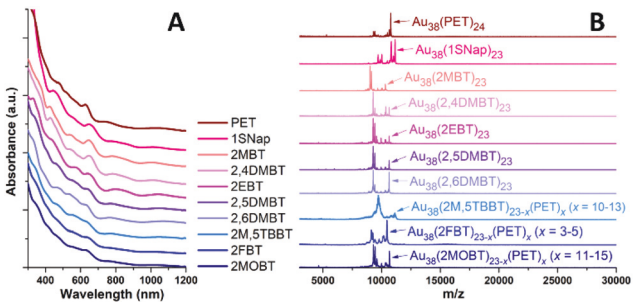

Fig. 1 (A) UV-vis spectra of different $Au_{38}(SR)_{24}$ NCs by ligand exchange on $Au_{38}(PET)_{24}$ with HSPh-X (X takes at least one *ortho*-position) at 45 °C and (B) the corresponding MALDI-MS spectra.

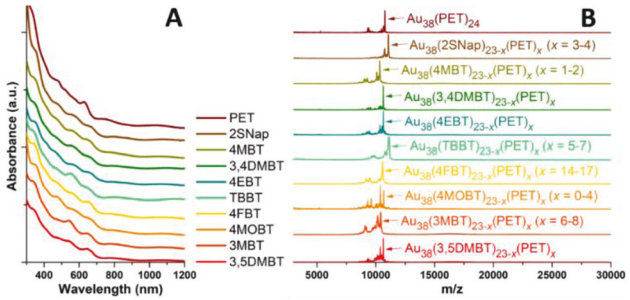

Fig. 2 (A) UV-vis spectra of different $Au_{38}(SR)_{24}$ NCs by ligand exchange on $Au_{38}(PET)_{24}$ with HSPh-X (X takes the *meta*- and/or *para*-position(s)) at RT and (B) the corresponding MALDI-MS spectra.

The absorption peak at the longest wavelength corresponds to the HOMO–LUMO gap for *para*- or *meta*-substituted benzenethiolate-protected Au_{38} and is observed to red-shift in all cases (Fig. S5†), indicating that the gap becomes smaller. It is worth noting that our results are different from the theoretical results that the *para*-substituents in $[Au_{25}(SPhX)_{18}]^-$ (X = H, F, Cl, Br, CH_3, and OCH_3) moderately shift the HOMO/LUMO energy states but without affecting the gap.[33]

2.3 Ligand exchange by cyclic thiols with no substituent

Finally, we investigate cyclic ligands such as non-conjugated cyclohexanethiol (CHT) and cyclopentanethiol (CPT), as well as conjugated benzenethiol (HSPh). The ligand exchange processes were also monitored at RT (Fig. S6†), and the resulting $Au_{38}(SPh)_{24}$ NCs were almost the same as reported previously,[34] except one or two PET ligands were left in the final product (Fig. 3).

It has been demonstrated that TBBT, CPT and SPh result in $Au_{36}(SR)_{24}$ at 80 °C.[21,34,35] Therefore, we repeated the ligand exchange process with HSPh-X (X takes *meta*- and/or *para*-site (s)) as well as with cyclic ligands at 80 °C (Fig. S7†). Except the *meta*-substituted benzenethiols and CHT, all other ligands gave $Au_{36}(SR)_{24}$ as the product due to ligand exchange-induced transformation. Only 4FBT and 4MOBT trials resulted in slightly incomplete ligand exchange (Fig. S8†).

Thus, it is also clear that although $Au_{38}(SR)_{24-x}(PET)_x$ retain the original structure at RT with partial ligand replacement, *meta*-substituted thiols cannot stabilize Au_{38} at 80 °C (decomposed), whereas *para*- or non-substituted benzenethiols drive the transformation from Au_{38} into Au_{36} as long as the thermodynamic barrier can be overcome. The case of 2,4DMBT was further tested at 80 °C as it has both *ortho*- and *para*-substituents, and pure $Au_{38}(2,4DMBT)_{24}$ was produced (Fig. S9†), indicating that *ortho*-substituents are more influential than other sites.

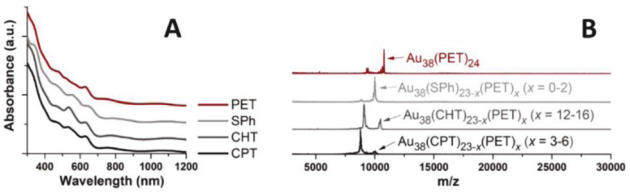

Fig. 3 (A) UV-vis spectra of different $Au_{38}(SR)_{24}$ NCs by ligand exchange on $Au_{38}(PET)_{24}$ with cyclic ligands at RT and (B) the corresponding MALDI-MS spectra.

2.4 $Au_{38}(2,4DMBT)_{24}$ *vs.* $Au_{38}(PET)_{24}$ structures

In our attempts to crystalize all the $Au_{38}(SR)_{24}$ NCs, only $Au_{38}(2MBT)_{24}$ and $Au_{38}(2,4DMBT)_{24}$ NCs were able to form single crystals (*via* diffusing methanol into dichloromethane solution of NCs over 2 days), but the crystal quality of $Au_{38}(2MBT)_{24}$ was not good enough. Only the crystal structure of $Au_{38}(2,4DMBT)_{24}$ was successfully determined by X-ray crystallography, which has also been reported recently by Wu's group.[36]

Similar to the crystal structure of the starting $Au_{38}(PET)_{24}$, $Au_{38}(2,4DMBT)_{24}$ also has a bi-icosahedral Au_{23} kernel, which is protected by three $Au(SR)_2$ motifs at the waist and six $Au_2(SR)_3$ motifs resembling two tri-blade fans at the top and bottom. However, the differences between the two NCs are obvious. The two tri-blade fans in $Au_{38}(PET)_{24}$ are arranged in a staggered conformation by ~60° to each other (Fig. 4A), while for $Au_{38}(2,4DMBT)_{24}$, one fan rotates only by ~45° relative to the other fan along the C_3 axis (Fig. 4B). Besides, each $Au(SR)_2$ motif is parallel to the two adjacent $Au_2(SR)_3$ motifs in $Au_{38}(2,4DMBT)_{24}$, but it is not so in the case of $Au_{38}(PET)_{24}$ (Fig. 4A and B, indicated by the blue lines). In addition, $Au_{38}(PET)_{24}$ is of C_1 symmetry and the NCs form a triclinic unit cell, whereas $Au_{38}(2,4DMBT)_{24}$ is of D_3 symmetry and the NCs are packed into a trigonal unit cell (Fig. 4C and D). This observation is consistent with our earlier observation that the

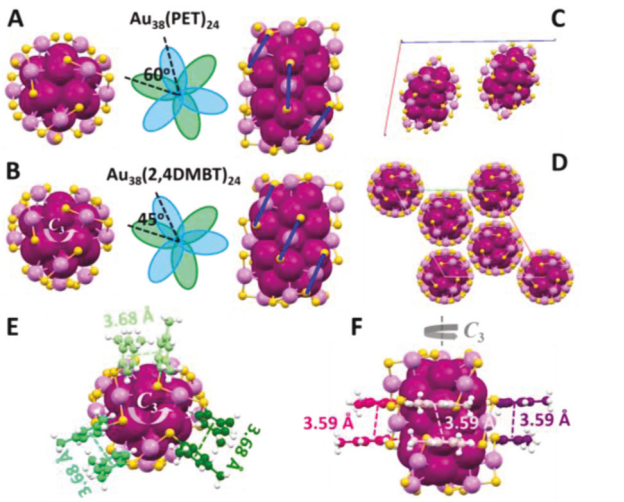

Fig. 4 Top/front view, and the schematic diagram of two overlapped tri-blade fans of (A) $Au_{38}(PET)_{24}$ and (B) $Au_{38}(2,4DMBT)_{24}$. (C) The triclinic unit cell of $Au_{38}(PET)_{24}$ and (D) the trigonal unit cell of $Au_{38}(2,4DMBT)_{24}$. The π···π interactions (E) in the same tri-blade fan and (F) in different tri-blade fans of $Au_{38}(2,4DMBT)_{24}$.

symmetry of NCs and the symmetry of the unit cell highly correlate.[14]

The changes in the arrangement of staple motifs and the symmetry of the NCs and unit cell are caused by the introduced new ligand. Significant π···π interactions in the solid state are observed between the 2,4DMBT ligands, *i.e.* the phenyl rings of the adjacent $Au_2(SR)_3$ motifs in the same tri-blade fan (Fig. 4E, three pairwise interactions marked in different greens, total six pairs) and those in different tri-blade fans (Fig. 4F, three pairwise interactions marked in different pinks). Such interactions on the surface of $Au_{38}(2,4DMBT)_{24}$ restrict the freedom of these motifs and improve the symmetry of the cluster. This can also be understood from the experimental perspective that heating (at least 45 °C, Fig. 1) is required for full ligand exchange with *ortho*-substituted benzenethiols as there is a thermodynamic barrier.

Despite the fact that strong π···π interactions could explain the high stability of $Au_{38}(2,4DMBT)_{24}$, one should understand that solvation in the solution phase might destroy π···π interactions. As we have discussed in sections 2.1–2.3, *ortho*-substituted benzenethiols act differently in stabilizing $Au_{38}(SR)_{24}$ compared to other thiols, hence there should be certain other interactions that are exclusive to the *ortho*-substituted SPh-X ligands. This led us to look into the possible Au···H–C interactions on the surface.[37] As shown in Fig. 5, such interactions are indeed found in $Au_{38}(2,4DMBT)_{24}$, as the H atoms of *ortho*-substituents are at substantially shorter distances to nearby Au atoms, including intra-motif interactions (marked in green in Fig. 5A and B) and inter-motif interactions (blue in Fig. 5A). All these interactions are within the ranges of d(Au···H) = 2.54–2.82 Å and ∠Au–H–C = 119.7–155.0°.

"Agostic" interactions of the type M···H–C were observed in many organometallic compounds with the M atoms from the early transition metals,[37] whereas the term "anagostic" was proposed to describe the M···H–C interactions for late transition elements.[38] The difference between "agostic" and "anagostic" interactions is based on M···H distances and M–H–C angles, and for the latter d(M···H) = 2.3–2.9 Å and ∠M–H–C = 110–170°.[38,39] Such interactions have been previously discussed in gold(I) complexes,[40–42] but rarely in Au NCs due to their typical geometry being unfavorable for such interactions.

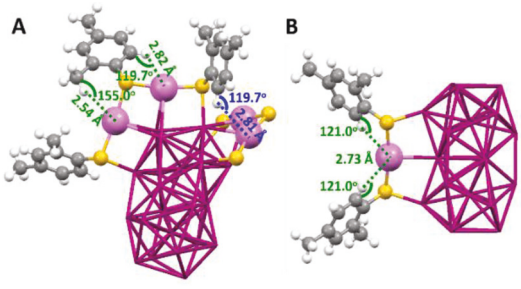

Fig. 5 The "anagostic" interactions between Au and H from (A) dimeric $Au_2(2,4DMBT)_3$ motif ligands and (B) the monomeric $Au(2,4DMBT)_2$ motif ligands.

Konishi *et al.* recently reported substantially short Au···H distances (d(M···H) ≈ 2.60–2.87 Å) in $[Au_6]^{2+}$, indicating that attractive interactions are critical to affect the stability of the cluster.[37] The observed d(Au···H) of 2.54–2.82 Å and ∠Au–H–C of 119.7–155.0° in $Au_{38}(2,4DMBT)_{24}$ are within the range of "anagostic" definition. Moreover, since the $Au_{38}(2,4DMBT)_{24}$ NC is of D_3 symmetry, there are totally six sets of interactions for the $Au_2(SR)_3$ motifs (only one set is shown in Fig. 5A), and all of the three $Au(SR)_2$ motifs (only one $Au(SR)_2$ is shown in Fig. 5B) can also form "anagostic" interactions on the surface of the NC.

In contrast, in the previously reported $Au_{38}(PET)_{24}$ structure, the shortest d(Au···H) was 2.96–3.26 Å and the corresponding ∠Au–H–C angles were 79.4–118.7°, which cannot be assigned to "anagostic" interactions (Fig. S10†). In other words, the average d(Au···H) in $Au_{38}(2,4DMBT)_{24}$ is significantly shortened by ~14% compared to that in $Au_{38}(PET)_{24}$, indicating much stronger surface Au···H interactions which contribute to the stability of the NC.[37] Thus, the *ortho*-substituents on benzenethiolates are critical for the formation of effective "anagostic" interactions.

Accordingly, the Au_{staple}–Au_{kernel} bond lengths of $Au_{38}(2,4DMBT)_{24}$ NCs are also affected by "anagostic" interactions, and the average bond length of 3.04 Å is 2.3% shorter than that of $Au_{38}(PET)_{24}$ (3.11 Å), indicating higher geometric stability for $Au_{38}(2,4DMBT)_{24}$.

2.5 TDDFT comparison of $Au_{38}(2,4DMBT)_{24}$ *vs.* $Au_{38}(PET)_{24}$

Based on the total structures of the two $Au_{38}(SR)_{24}$ NCs, we are able to gain more insights into their electronic structures. In our TDDFT, we retain the crystal symmetries of the NCs and the full ligands are incorporated into the calculations (Fig. S11†). The local projected density of states (LPDOS) per atom is shown in Fig. S12.† For both $Au_{38}(SR)_{24}$ NCs, the density of states is mainly delocalized over the $Au_{38}S_{24}$ frame. However, it is clear that in the case of $Au_{38}(2,4DMBT)_{24}$, the local p states of C atoms significantly contribute to the frontier molecular orbitals (*i.e.* HOMO−4 to LUMO+4), while for $Au_{38}(PET)_{24}$, the carbon contribution is almost negligible (Fig. S12†).

The Kohn–Sham (KS) diagrams of the HOMO and LUMO for the two Au_{38} NCs are shown in Fig. 6, and more frontier orbitals can be found in Fig. S13.† The diagrams of $Au_{38}(2,4DMBT)_{24}$ (Fig. 6A and Fig. S13A†) are well consistent

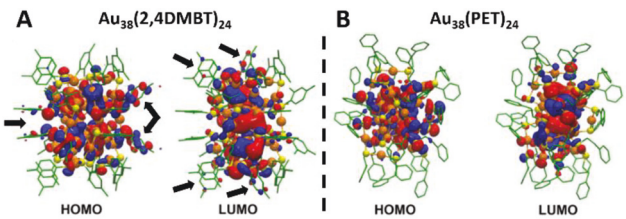

Fig. 6 The Kohn–Sham diagrams of the HOMO and LUMO for (A) $Au_{38}(2,4DMBT)_{24}$ and (B) $Au_{38}(PET)_{24}$ NCs.

with the reports by Aikens and co-workers on $Au_{38}(SH)_{24}$ and $Au_{38}(SCH_3)_{24}$ of D_3 symmetry.[43,44] As for the frontier orbitals near the HOMO–LUMO gap of $Au_{38}(PET)_{24}$, the orbital symmetry is less well-defined (Fig. 6B and Fig. S13B†) compared to that of $Au_{38}(2,4DMBT)_{24}$ in which Σ, Π and Δ character can be clearly identified (Fig. 6A and Fig. S13A†). More importantly, for HOMO−2 to LUMO+2 orbitals, it is visualized that the electron density is even delocalized from the $Au_{38}S_{24}$ frame to the aromatic rings of 2,4DMBT (Fig. 6A black arrows, Fig. S13A†), while no electron density can be found on the $-CH_2CH_2Ph$ groups (Fig. 6B and Fig. S13B†).

It has been reported that for Au NCs protected by terminal alkynyls, as Au kernel and R groups could be coupled *via* C≡C, the frontier MOs and optical properties would be affected in a more profound way than in Au-SR NCs.[45] In alkynyl-protected Au_{25}, the C(*p*) character of alkyne ligands is found to be mainly involved in high-energy transitions, but only slightly affects the HOMO–LUMO transition.[46] In contrast, the π···π stacking of phenyl rings in the $Au_{38}(2,4DMBT)_{24}$ solid state results in meaningful differences in the electronic structure, especially the HOMO and LUMO as well as the adjacent orbitals.

The simulated optical spectra of both $Au_{38}(SR)_{24}$ NCs are shown in Fig. S14A and B.† Except the slightly blue-shifted peak **a** (HOMO/HOMO−1 to LUMO/LUMO+1 transitions), all other peaks **b**/**c**/**d** of $Au_{38}(2,4DMBT)_{24}$ are red-shifted by ~0.1–0.2 eV with respect to the corresponding peaks **a′**/**b′**/**c′**/**d′** of $Au_{38}(PET)_{24}$. The electronic transitions contributing to these main absorption peaks (**a**/**b**/**c**/**d** or **a′**/**b′**/**c′**/**d′**) are given in Table S1.† In both NCs, the HOMO and HOMO−1 are nearly degenerated, whereas the LUMO and LUMO+1 are closer for $Au_{38}(2,4DMBT)_{24}$ compared to $Au_{38}(PET)_{24}$ (Fig. S14C and Table S2†). This is reflected in experimental spectra by a slightly larger energy gap, *i.e.* blue-shifted peak **a** (Fig. S14A†). On the other hand, the energy difference between the HOMO−1 and HOMO−2 increases from 0.162 eV in $Au_{38}(2,4DMBT)_{24}$ to 0.331 eV in $Au_{38}(PET)_{24}$. This explains the obvious shifts of peaks **b**/**c**/**d** to lower energies for $Au_{38}(2,4DMBT)_{24}$, and a shoulder in peak **b** (Fig. S14A,† blue arrow) due to peak splitting. The overall higher energy states for $Au_{38}(2,4DMBT)_{24}$ compared to $Au_{38}(PET)_{24}$ (Fig. S14C,† indicated by the blue dashed arrows), especially the much higher HOMO−2, suggest less electronic stability, although the two NCs have similar energy gaps.

This observation that $Au_{38}(PET)_{24}$ is more electronically stable in above theoretical analysis led us to check the atomic charges of the two clusters (Table S3†). The average atomic charges of metal atoms in $Au_{38}(PET)_{24}$ are slightly less positive (by 0.46*e* per Au_{38}) than those in $Au_{38}(2,4DMBT)_{24}$. However, the S atoms in $Au_{38}(PET)_{24}$ hold much more negative charge (by −1.41*e* more per S_{24}) than in $Au_{38}(2,4DMBT)_{24}$. This greater electron-withdrawing effect of S atoms in $Au_{38}(PET)_{24}$ can be attributed to the enhanced stability of its molecular orbitals of HOMO−2 and lower ones, resulting in the blue-shift of absorption peaks **b′**/**c′**/**d′** (Fig. 7A and B), which is consistent with the calculations on Au_{38} previously reported.[24]

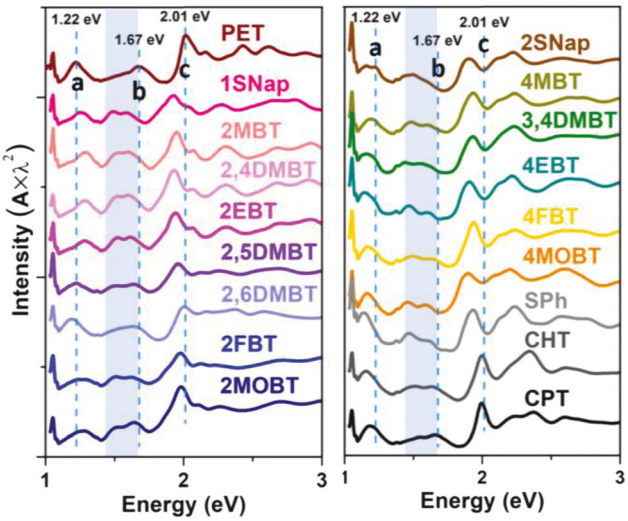

Fig. 7 Cryogenic UV-vis-NIR spectra (80 K) of different $Au_{38}(SR)_{24}$ NCs. The dashed lines indicate the absorption peak positions of $Au_{38}(PET)_{24}$ at 80 K.

The question is, if $Au_{38}(SPh\text{-}X)_{24}$ NCs (aromatic thiolates as the stabilizer) are less electronically stable than $Au_{38}(PET)_{24}$ (non-aromatic stabilizer), why can they sustain the harsh ligand exchange conditions of 80 °C? We rationalize that the π···π interactions in the solid state, and more importantly, the distinctive "anagostic" Au···H–C interactions on the surface (see section 2.4) should largely improve the geometric stability and effectively offset the loss in electronic stability.

2.6 Summary on the ligand exchange of $Au_{38}(PET)_{24}$

A summary on the ligand exchange of $Au_{38}(PET)_{24}$ is given in Table 1. Complete ligand exchange with *ortho*-substituted SPh-X cannot be carried out on Au_{38} at RT, but requires higher temperatures; ligand exchange with other ligands without an *ortho*-substituent cannot be completed on Au_{38} at RT except for SPh (almost complete), while at high temperatures, structural transformation into Au_{36} is inevitable, if not decomposed.

The cryogenic optical absorption spectra of $Au_{38}(SR)_{24}$ NCs after ligand exchange were measured at 80 K in 2-methyltetrahydrofuran (Fig. 7). All the peaks become more prominent with blue-shifts compared to those at room temperature. The spectrum of $Au_{38}(PET)_{24}$ is well consistent with the literature.[47] Besides, the spectrum of $Au_{38}(SPh)_{24}$ at low temperatures also agrees with the reported data.[34] Generally, after ligand exchange, peaks **b**/**c** of the resulted Au_{38} all shift to lower energies, especially those capped by aromatic ligands, and there is a unanimous splitting in peak **b** (shaded region, Fig. 7). Such a peak splitting is consistent with the calculated split transitions (Fig. S14C†). We also noted that for Au_{38} NCs protected by *ortho*-substituted SPh-X, the absorption peaks at the lowest energy (peak **a**) are generally blue-shifted compared to those for the $Au_{38}(PET)_{24}$, while for other Au_{38} NCs protected by ligands without *ortho*-substituents, the corresponding peaks **a**

Table 1 Summary of ligand exchange on $Au_{38}(PET)_{24}$ at different temperatures, and the lowest energy absorption peak positions of the ligand-exchanged Au_{38} (tested at 295 K and 80 K)

Ref.	PET	RT	45 °C	80 °C	Au_{38} 295 K (eV)	Au_{38} 80 K (eV)
					1.22	1.19
Ortho-	1SNap	→	√	√	1.25	1.22
	2MBT	→	√	√	1.29	1.23
	2,4DMBT	—	√	√	1.28	1.22
	2EBT	—	√	—	1.28	1.18
	2,5DMBT	—	√	—	1.22	1.18
	2,6DMBT	—	√	—	1.19	1.15
	2M,5TBBT	—	→	→	1.19	—
	2FBT	—	→	→	1.24	1.20
	2MOBT	—	→	→	1.24	1.20
Para-	2SNap	→	—	Δ	1.16	1.14
	4MBT	→	—	Δ	1.19	1.16
	3,4DMBT	→	—	Δ	1.16	1.12
	4EBT	→	—	Δ	1.15	1.15
	TBBT	→	—	Δ (ref. 21)	1.07	—
	4FBT	→	—	Δ	1.17	1.15
	4MOBT	→	—	Δ	1.16	1.14
Meta-	3MBT	→	—	×	1.12	—
	3,5MBT	→	—	×	1.14	—
Cyclic-	SPh	√	—	Δ	1.14	1.12
	CHT	→	—	×	1.16	1.12
	CPT	→	—	Δ (ref. 35)	1.18	1.13

→ incomplete ligand exchange; √ complete ligand exchange; Δ structural transformation; × decomposed; and — not performed.

are all clearly red-shifted (Table 1 and Fig. 7). The conformance in optical properties related to the substituent sites implies that the *ortho*-substituents on benzenethiolates play a critical role in the stability of Au_{38} by forming additional "anagostic" interactions on the NC surface, while the *para*-substituents drive the structural transformation into Au_{36}.

3. Conclusions

In summary, in order to understand the ligand preference for specific size Au-SR NCs, we have performed detailed ligand exchanges on $Au_{38}(PET)_{24}$ with as many as 21 different incoming thiols. It is clear that the *ortho*-substituted SPh-X retains the structure of $Au_{38}(SR)_{24}$, while the *para*- or non-substituted SPh(X) causes the transformation into $Au_{36}(SR)_{24}$. Strong electron-donating or -withdrawing groups do not make any difference, but hamper full ligand exchange. Our study on the crystal structure of $Au_{38}(2,4DMBT)_{24}$ identifies distinctive π···π interactions, and more importantly the "anagostic" interactions which are rare in nanoclusters, and interestingly both types of interactions are absent in $Au_{38}(PET)_{24}$. TDDFT shows that for aromatic ligand-protected Au_{38}, the electron density extends from the Au–S frame to the ligands, and the peaks in the visible region red-shift due to the much increased HOMO−2 energy, indicating decreased electronic stability. However, this destabilization is effectively compensated for by the "anagostic" interactions observed in Au_{38} protected with the *ortho*-substituted SPh, which enhance the geometric stability of $Au_{38}(2,4DMBT)_{24}$.

Conflicts of interest

There are no conflicts to declare.

Acknowledgements

We acknowledge financial support from the National Science Foundation (NSF DMR-1808675 and CBET-CAREER program under Grant No. 1652694). Computational support was provided by the Center for Research Computing (CRC) at the University of Pittsburgh as well as the Extreme Science and Engineering Discovery Environment (XSEDE), which is supported by the NSF (ACI-1548562).

Notes and references

1 R. Jin, C. Zeng, M. Zhou and Y. Chen, *Chem. Rev.*, 2016, **116**, 10346.
2 I. Chakraborty and T. Pradeep, *Chem. Rev.*, 2017, **117**, 8208.
3 Y. Negishi, Y. Takasugi, S. Sato, H. Yao, K. Kimura and T. Tsukuda, *J. Am. Chem. Soc.*, 2004, **126**, 6518.
4 Y. Negishi, K. Nobusada and T. Tsukuda, *J. Am. Chem. Soc.*, 2005, **127**, 5261.
5 H. Tsunoyama and T. Tsukuda, *J. Am. Chem. Soc.*, 2009, **131**, 18216.
6 M. Zhu, C. M. Aikens, F. J. Hollander, G. C. Schatz and R. Jin, *J. Am. Chem. Soc.*, 2008, **130**, 5883.
7 H. Qian, Y. Zhu and R. Jin, *ACS Nano*, 2009, **3**, 3795.
8 H. Qian, W. T. Eckenhoff, Y. Zhu, T. Pintauer and R. Jin, *J. Am. Chem. Soc.*, 2010, **132**, 8280.
9 S. Chen, S. Wang, J. Zhong, Y. Song, J. Zhang, H. Sheng, Y. Pei and M. Zhu, *Angew. Chem., Int. Ed.*, 2015, **54**, 3145.
10 A. Das, C. Liu, H. Y. Byun, K. Nobusada, S. Zhao, N. L. Rosi and R. Jin, *Angew. Chem., Int. Ed.*, 2015, **54**, 3140.
11 C. Zeng, Y. Chen, K. Iida, K. Nobusada, K. Kirschbaum, K. J. Lambright and R. Jin, *J. Am. Chem. Soc.*, 2016, **138**, 3950.
12 T. C. Jones, L. Sumner, G. Ramakrishna, M. bin Hatshan, A. Abuhagr, S. Chakraborty and A. Dass, *J. Phys. Chem. C*, 2018, **122**, 17726.
13 H. Yang, Y. Wang, J. Yan, X. Chen, X. Zhang and H. Häkkinen, *J. Am. Chem. Soc.*, 2014, **136**, 7197.
14 Y. Li, T.-Y. Luo, M. Zhou, Y. Song, N. L. Rosi and R. Jin, *J. Am. Chem. Soc.*, 2018, **140**, 14235.
15 P. J. Krommenhoek, J. Wang, N. Hentz, A. C. Johnston-Peck, K. A. Kozek, G. Kalyuzhny and J. B. Tracy, *ACS Nano*, 2012, **6**, 4903.
16 Y. Chen, C. Zeng, D. R. Kauffman and R. Jin, *Nano Lett.*, 2015, **15**, 3603.
17 H. Yang, Y. Wang and N. Zheng, *Nanoscale*, 2013, **5**, 2674.

18 J. Chai, S. Yang, Y. Lv, T. Chen, S. Wang, H. Yu and M. Zhu, *J. Am. Chem. Soc.*, 2018, **140**, 15582.
19 T. Higaki, M. Zhou, K. J. Lambright, K. Kirschbaum, M. Y. Sfeir and R. Jin, *J. Am. Chem. Soc.*, 2018, **140**, 5691.
20 C. Zeng, Y. Chen, K. Kirschbaum, K. Appavoo, M. Y. Sfeir and R. Jin, *Sci. Adv.*, 2015, **1**, e1500045.
21 C. Zeng, C. Liu, Y. Pei and R. Jin, *ACS Nano*, 2013, **7**, 6138.
22 C. Zeng, T. Li, A. Das, N. L. Rosi and R. Jin, *J. Am. Chem. Soc.*, 2013, **135**, 10011.
23 Q. Shi, Z. Qin, C. Yu, S. Liu, H. Xu and G. Li, *Nanoscale*, 2020, **12**, 4982.
24 J. Jung, S. Kang and Y.-K. Han, *Nanoscale*, 2012, **4**, 4206.
25 J. Zhong, X. Tang, J. Tang, J. Su and Y. Pei, *J. Phys. Chem. C*, 2015, **119**, 9205.
26 Y. Chen, C. Liu, Q. Tang, C. Zeng, T. Higaki, A. Das, D.-E. Jiang, N. L. Rosi and R. Jin, *J. Am. Chem. Soc.*, 2016, **138**, 1482.
27 Q. Tang, R. Ouyang, Z. Tian and D.-E. Jiang, *Nanoscale*, 2015, **7**, 2225.
28 A. Das, T. Li, G. Li, K. Nobusada, C. Zeng, N. L. Rosi and R. Jin, *Nanoscale*, 2014, **6**, 6458.
29 L. Cheng, C. Ren, X. Zhang and J. Yang, *Nanoscale*, 2013, **5**, 1475.
30 X. Nie, C. Zeng, X. Ma, H. Qian, Q. Ge, H. Xu and R. Jin, *Nanoscale*, 2013, **5**, 5912.
31 B. Molina, A. Sánchez-Castillo, S. Knoppe, I. L. Garzón, T. Bürgi and A. Tlahuice-Flores, *Nanoscale*, 2013, **5**, 10956.
32 Y. Li, Y. Chen, S. D. House, S. Zhao, Z. Wahab, J. C. Yang and R. Jin, *ACS Appl. Mater. Interfaces*, 2018, **10**, 29425.
33 C. M. Aikens, *J. Phys. Chem. Lett.*, 2010, **1**, 2594.
34 M. Rambukwella, S. Burrage, M. Neubrander, O. Baseggio, E. Aprà, M. Stener, A. Fortunelli and A. Dass, *J. Phys. Chem. Lett.*, 2017, **8**, 1530.
35 A. Das, C. Liu, C. Zeng, G. Li, T. Li, N. L. Rosi and R. Jin, *J. Phys. Chem. A*, 2014, **118**, 8264.
36 S. Zhuang, L. Liao, J. Yuan, N. Xia, Y. Zhao, C. Wang, Z. Gan, N. Yan, L. He, J. Li, H. Deng, Z. Guan, J. Yang and Z. Wu, *Angew. Chem., Int. Ed.*, 2019, **58**, 4510.
37 M. A. Bakar, M. Sugiuchi, M. Iwasaki, Y. Shichibu and K. Konishi, *Nat. Commun.*, 2017, **8**, 576.
38 M. Brookhart, M. L. H. Green and G. Parkin, *Proc. Natl. Acad. Sci. U. S. A.*, 2007, **104**, 6908.
39 W. I. Sundquist, D. P. Bancroft and S. J. Lippard, *J. Am. Chem. Soc.*, 1990, **112**, 1590.
40 H. Schmidbaur, H. G. Raubenheimer and L. Dobrzańska, *Chem. Soc. Rev.*, 2014, **43**, 345.
41 H. Schmidbaur, *Angew. Chem., Int. Ed.*, 2019, **58**, 5806.
42 M. Rigoulet, S. Massou, E. D. Sosa Carrizo, S. Mallet-Ladeira, A. Amgoune, K. Miqueu and D. Bourissou, *Proc. Natl. Acad. Sci. U. S. A.*, 2019, **116**, 46.
43 O. Lopez-Acevedo, H. Tsunoyama, T. Tsukuda, H. Häkkinen and C. M. Aikens, *J. Am. Chem. Soc.*, 2010, **132**, 8210.
44 K. L. D. M. Weerawardene, E. B. Guidez and C. M. Aikens, *J. Phys. Chem. C*, 2017, **121**, 15416.
45 N. Kobayashi, Y. Kamei, Y. Shichibu and K. Konishi, *J. Am. Chem. Soc.*, 2013, **135**, 16078–16081.
46 J.-J. Li, Z.-J. Guan, Z. Lei, F. Hu and Q.-M. Wang, *Angew. Chem., Int. Ed.*, 2019, **58**, 1083.
47 M. S. Devadas, S. Bairu, H. Qian, E. Sinn, R. Jin and G. Ramakrishna, *J. Phys. Chem. Lett.*, 2011, **2**, 2752.